

# Fine Timing and Frequency Synchronization for MIMO-OFDM: An Extreme Learning Approach

Jun Liu, Kai Mei, Xiaochen Zhang, Des McLernon, *Member, IEEE*, Dongtang Ma, *Senior Member, IEEE*, Jibo Wei, *Member, IEEE* and Syed Ali Raza Zaidi, *Senior Member, IEEE*

**Abstract**—Multiple-input multiple-output orthogonal frequency-division multiplexing (MIMO-OFDM) is a key technology component in the evolution towards next-generation communication in which the accuracy of timing and frequency synchronization significantly impacts the overall system performance. In this paper, we propose a novel scheme leveraging extreme learning machine (ELM) to achieve high-precision timing and frequency synchronization. Specifically, two ELMs are incorporated into a traditional MIMO-OFDM system to estimate both the residual symbol timing offset (RSTO) and the residual carrier frequency offset (RCFO). The simulation results show that the performance of an ELM-based synchronization scheme is superior to the traditional method under both additive white Gaussian noise (AWGN) and frequency selective fading channels. Finally, the proposed method is robust in terms of choice of channel parameters (e.g., number of paths) and also in terms of "generalization ability" from a machine learning standpoint.

**Index Terms**—Extreme learning machine, timing, frequency synchronization, MIMO-OFDM, frequency selective fading.

## I. INTRODUCTION

FIFTH generation (5G) cellular communications technology for commercial use is currently being deployed in various countries. Meanwhile, research into sixth generation (6G) systems is already under way as it is designed to meet the needs of ultra-high capacity, reliability and low latency [1]. Among existing and future technologies, multiple-input multiple-output orthogonal frequency-division multiplexing (MIMO-OFDM) will continue to play an important role that facilitates development and deployment. As an effective physical layer solution, the spectral efficiency (SE) of OFDM systems is superior to conventional single carrier systems and it can combat inter-symbol interference (ISI) through transforming a frequency-selective fading channel into many parallel flat-fading subchannels.

However, OFDM systems are highly sensitive to carrier frequency offset (CFO) which can destroy the important orthogonality between subcarriers and this results in the degradation of bit error rate (BER) performance. Therefore, the estimation

of accurate CFO is crucial to OFDM systems. Meanwhile, symbol timing offset (STO) can result in ISI and a rotated phase whose value is proportional to the subcarrier index at the FFT output in an OFDM receiver.

The traditional approach towards the estimation of both STO (also known as the timing synchronization) and CFO (also known as the frequency synchronization), involves sending a preamble at OFDM transmitters and processing the signals at the receivers. These signal processing techniques have been studied extensively, and many seminal articles have been published since the 1990s. P.H. Moose addressed the issue of receiver frequency synchronization by proposing an algorithm for a maximum likelihood estimate (MLE) of the CFO using the discrete Fourier transform (DFT) of a repeated symbol, and a lower bound for signal-to-noise (SNR) has been derived [2]. In [3], a method for the rapid and robust frequency and timing synchronization for OFDM has been presented by Schmidl *et al.* Then, an implementation of an MIMO-OFDM-based wireless local area network (WLAN) system was demonstrated by [4], in which a simple MIMO extension of Schmidl's algorithm [3] proposed in [5] is deployed in a practical system. In [6] the authors address the problem of training design for a frequency-selective channel and also CFO estimation in single- and multiple-antenna systems under different energy-distribution constraints. In [7] and [8], a new framework referred to as sparse blind CFO estimation for interleaved uplink orthogonal frequency-division multiple access (OFDMA) and the sparse recovery assisted CFO estimator for the uplink OFDMA were respectively proposed. Timing and frequency synchronization, as well as channel estimation can be carried out jointly to achieve better performance. [9] presents a novel preamble-aided method for joint estimation of timing, carrier frequency offset, and channel parameters for OFDM. [10] considered the joint maximum likelihood estimator for the channel impulse response (CIR) and the CFO. In [11], a comprehensive literature review and classification of the recent research progress in timing and carrier synchronization was presented.

But, errors will nearly always remain in the estimation of STO and CFO, which are also known as residual STO (RSTO) and residual CFO (RCFO). This is due to the effects of fading and thermal noise. The influence of STO errors on channel interpolation is analyzed in [12]. Even a small RCFO can result in amplitude and phase distortion and also inter-carrier interference (ICI) among subcarriers. Traditionally, in order to mitigate the impact of RCFO, channel tracking methods are employed, and this is realized by inserting known

This work was supported in part by the China Scholarship Council (CSC), National Natural Science Foundation of China (NSFC) under Grant 61931020, 61372099 and 61601480. (*Corresponding author: Dongtang Ma and Jun Liu.*)

Jun Liu, Kai Mei, Xiaochen Zhang, Dongtang Ma, and Jibo Wei are with the College of Electronic Science and Technology, National University of Defense Technology, Changsha 410073, China (E-mail: {liujun15, meikai11, zhang-xiaochen14, dongtangma, wjbhw}@nudt.edu.cn).

Des McLernon, Jun Liu and Syed Ali Raza Zaidi are with the School of Electronic and Electrical Engineering, University of Leeds, Leeds, LS2 9JT, UK (E-mail: {D.C.McLernon, eljliu, S.A.Zaidi}@leeds.ac.uk).

pilots into specific subcarriers. However, this method reduces system SE. As regards RSTO, compensation method for channel correction need to be used. To reduce the sensitivity to synchronization errors, [13] develops conditions for the selection of appropriate Zadoff-Chu sequences.

In recent years, challenges to traditional methods have emerged that use by the data-based approaches relying on machine learning [14]–[17]. A popular scheme is machine learning-based end-to-end communications systems. Basing on the idea of autoencoder, Dörner *et al.* proposed a learning-based communication system, in which the task of synchronization is addressed through a neural network [18]. Similarly, in [19], a sampling time synchronization model using a convolutional neural network (CNN) for end-to-end communications systems is introduced. In [20], an extreme learning machine (ELM)-based frame synchronization method for a burst-mode communication system was proposed. Finally, [21] investigates a deep neural network (DNN)-based solution for packet detection and CFO estimation.

Although the above-mentioned machine learning-based schemes achieve better performance or robustness than traditional methods, their shortcomings lead to serious difficulties in practical implementation. We summarize the challenges and deficiencies of these schemes as follows.

- In previous machine learning related works, synchronization technique is ignored and perfect synchronization is assumed. Since the trained parameters of the neural network depend highly on the input data, when the test signal has STO and CFO, these methods would crash.
- The mathematical theory of communication was exhaustively explored by Shannon in [22], where the fundamental problem of communication is described as “reproducing at one point either exactly or approximately a message selected at another point”. But, autoencoder-based methods [18], [19] present a “chicken and egg” problem, because significant “known information” is actually necessary to train the autoencoder thus making it impractical.
- So, most of the previous works sink into this paradox of the “chicken or the egg” causality dilemma [18]–[21]. Specifically, in the training stage, labeled data with exact timing location and CFO under given channel models are necessary. Unfortunately, it is impossible to acquire labeled data under real channel environments.
- The common disadvantage of most of the current learning-based techniques lies in the computational complexity because they are based on a DNN. DNNs usually have deep hidden layers, which requires prohibitive computational complexity. Even when an ELM-based scheme with only one hidden layer is applied in [20], a significant training data under a given channel realization is indispensable.

Motivated by the causality “chicken or the egg” dilemma and the prohibitive computational complexity in machine learning-based schemes, in this paper we first propose a robust ELM-based fine timing and frequency synchronization scheme to deal with the challenges above. The main contributions of

this paper are summarized as follows.

- For MIMO-OFDM, we incorporate ELM with a traditional STO estimator. The fine timing synchronization can be carried out by ELM without the need for any prior information about the channel.
- We first propose a robust ELM-based scheme to realize RCFO estimation without the need for additional prior information, where the ELM can learn the mapping relationship between the preamble corrupted by both RSTO and RCFO.
- We provide a performance analysis of the proposed learning scheme in different cases. Specifically, computer simulation results show that the proposed scheme is superior to traditional STO and CFO estimation methods in terms of mean squared error (MSE). Also, extensive simulation results and comparisons have demonstrated the robustness and (machine learning) generalization ability of the proposed scheme. Finally, we give the complexity analysis of the complex ELM and DNN methods.

The remainder of this paper is organized as follows. The signal model of the MIMO-OFDM system and traditional timing and frequency synchronization for MIMO-OFDM are presented in Sections II and III, respectively. In Section IV, we propose a scheme that incorporates ELM into the traditional MIMO-OFDM system, in which ELM is used to estimate RSTO and RCFO. Then, numerical results and analysis for evaluating the performance of the proposed scheme are provided in Section V, which is followed by conclusions in Section VI.

*Notations:* The notations adopted in the paper are as follows. We use boldface lowercase  $\mathbf{x}$  and capital letters  $\mathbf{X}$  to denote column vectors and matrices, respectively. Superscripts  $^{-1}$ ,  $*$ ,  $T$ ,  $H$  and  $\dagger$  stand for inverse, conjugate, transpose, Hermitian transpose and Moore-Penrose generalized matrix inverse, respectively.  $\otimes$ ,  $\odot$ ,  $\circledast$ ,  $E\{\cdot\}$ ,  $[\cdot]$  and  $j = \sqrt{-1}$  denote Kronecker product, Hadamard product, cyclic convolution, the expectation operation, floor function and the imaginary unit. Note that  $\angle(\cdot)$  returns the phase angle of a complex number. Finally,  $\text{repmat}(\mathbf{A}, m, n)$  returns an array containing  $m$  and  $n$  copies of  $\mathbf{A}$  in the column and row dimensions, respectively.

## II. MIMO-OFDM SIGNAL MODEL

Let us consider a MIMO-OFDM system with  $N_t$  transmit (TX) and  $N_r$  receive (RX) antennas, which is usually denoted as a  $N_t \times N_r$  system. Without loss of generality, we consider the frequency-domain MIMO-OFDM signal model, which is directly given as [4]

$$\tilde{\mathbf{x}}(a) = \tilde{\mathbf{H}}\tilde{\mathbf{s}}(a) + \tilde{\mathbf{n}}(a) \quad (1)$$

where an  $N_r N_c$ -dimensional complex vector  $\tilde{\mathbf{x}}(a)$  represents the frequency-domain received signal,  $\tilde{\mathbf{s}}(a) = [\mathbf{s}(0, a)^T \cdots \mathbf{s}(N_c - 1, a)^T]^T \in^{N_r N_c \times 1}$  and  $\mathbf{s}(k, a)$  represents an  $N_r$ -dimensional complex vector transmitted on the  $k$ th subcarrier of the  $a$ th MIMO-OFDM symbol with  $S_p(k, a)$  is its  $p$ th element, i.e., transmitted on the  $p$ th TX antenna.  $\tilde{\mathbf{n}}(a)$  represents the frequency-domain noise vector, with i.i.d. zero-mean, complex Gaussian elements with variance  $0.5\sigma_n^2$  per

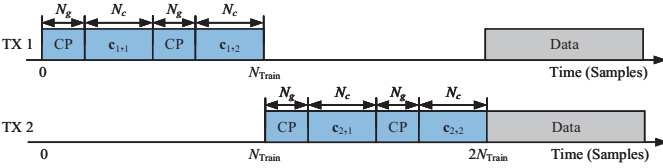


Fig. 1. Structure of a time orthogonal preamble for a  $2 \times 2$  MIMO-OFDM system.

dimension, and the channel frequency response is represented as a block diagonal matrix  $\tilde{\mathbf{H}}$  as follows:

$$\tilde{\mathbf{H}} = \begin{bmatrix} \mathbf{H}(0) & & 0 \\ & \ddots & \\ 0 & & \mathbf{H}(N_c - 1) \end{bmatrix}. \quad (2)$$

Now,  $\mathbf{H}(k) \in \mathbb{C}^{N_r \times N_t}$  represents the  $N_t \times N_r$  MIMO channel for the  $k$ th subcarrier and can be shown to be

$$\mathbf{H}(k) = \sum_{l=0}^{L-1} \mathbf{G}(l) \exp\left(-j2\pi \frac{kl}{N_c}\right). \quad (3)$$

where  $l$ th path of MIMO CIR matrix  $\mathbf{G}(l) \in \mathbb{C}^{N_r \times N_t}$  and its  $(q, p)$ th element is  $g_{q,p}(l)$ . We assume that these taps are independent, zero-mean, complex Gaussian random variables with variance  $0.5P_l$  per dimension. The ensemble  $P_l$ ,  $l = \{0, \dots, L-1\}$  is called the power delay profile (PDP) and its total power is assumed to be normalized to  $\sigma_c^2 = 1$ . For each  $k$ th subcarrier, the signal model can be written in its flat-fading form as

$$\mathbf{x}(k, a) = \mathbf{H}(k) \mathbf{s}(k, a) + \mathbf{n}(k, a). \quad (4)$$

### III. TRADITIONAL TIMING AND FREQUENCY SYNCHRONIZATION FOR MIMO-OFDM

We consider the traditional preamble pattern [3] and synchronization method [4] in this section. As shown in Fig. 1, in order to estimate the subchannels between the different TX and RX antennas, a time orthogonal preamble is chosen. The length of the preamble for all the TX antennas is  $N_{\text{train}} = N_g + N_c$ , where  $N_g$  and  $N_c$  denote the length of the cyclic prefix (CP) and one OFDM symbol, respectively.  $\mathbf{c}_{p,1}$  and  $\mathbf{c}_{p,2}$  are different pseudo-noise (PN) sequences transmitted by the  $p$ th TX.

The first part of the preamble  $\mathbf{c}_{p,1}$  comprises two identical halves in the time domain, which is used for symbol timing and fractional CFO estimation. This kind of time-domain identical structure can be obtained by transmitting a PN sequence only on the even frequencies while zeros are placed on the odd frequencies. The second part of the preamble  $\mathbf{c}_{p,2}$  contains a PN sequence on its odd frequencies to measure these subchannels and another PN sequence on the even frequencies to help determine the frequency offset.

#### A. Timing Synchronization

Before the estimation of CFO is conducted, the STO ( $\tau$ ) needs to be estimated. The method for timing synchronization is given by

$$\hat{\tau} = \underset{d}{\operatorname{argmax}} \frac{1}{N_g} \sum_{m=0}^{N_g-1} \left[ \frac{\sum_{p=1}^{N_t} |\Lambda(d_p + m)|^2}{\sum_{p=1}^{N_t} P(d_p + m)^2} \right], \quad (5)$$

where  $d_p = d - (N_t - p) N_{\text{train}}$  and  $d$  is discrete variable.  $\Lambda(d)$  is complex correlation of the first part of preamble  $\mathbf{c}_1$ , and is given by

$$\Lambda(d) = \sum_{i=d-(N_c/2-1)}^d \sum_{q=1}^{N_r} r_q^*(i - N_c/2) r_q(i) \quad (6)$$

and  $r_q(i)$  is the  $i$ th sample of the received signal on the  $q$ th antenna. The received energy for the second half-symbol of  $\mathbf{c}_1$ ,  $P(d)$ , is defined by

$$P(d) = \sum_{i=d-(N_c/2-1)}^d \sum_{q=1}^{N_r} r_q^*(i) r_q(i). \quad (7)$$

Note that  $d$  is a time index corresponding to the first sample in a window of  $N_c$  samples.  $\frac{1}{N_g} \sum_{m=0}^{N_g-1} (\cdot)$  is  $N_g$ -point moving average.

#### B. Frequency Synchronization

In this subsection, the CFO estimation method is based on [3]. We define normalized CFO,  $\varepsilon$ , as a ratio of the CFO  $f_{\text{offset}}$  to subcarrier spacing  $\Delta f$ , shown as  $\varepsilon = f_{\text{offset}}/\Delta f$ . Let  $\varepsilon_i$  and  $\varepsilon_f$  denote the integer part and fractional part of  $\varepsilon$ , respectively, and therefore  $\varepsilon = \varepsilon_i + \varepsilon_f$ , where  $\varepsilon_i = \lfloor \varepsilon \rfloor$ . If  $|\varepsilon| \leq 1$ , the CFO can be estimated directly as

$$\hat{\varepsilon} = \frac{\hat{\theta}}{\pi} = \frac{\angle \left[ \sum_{p=1}^{N_t} \Lambda(\hat{\tau}) \right]}{\pi}, \quad (8)$$

where  $\hat{\theta}$  denotes the phase of the summation of the complex correlations of the preambles originating from the different transmitters. When  $|\varepsilon| > 1$ , the PN sequence on the even frequencies of  $\mathbf{c}_2$  will be needed and the CFO can be given by

$$\varepsilon = \frac{\theta}{\pi} + 2g, \quad (9)$$

where  $g$  is an integer. By partially correcting the frequency offset, adjacent carrier interference can be avoided, and then the remaining offset of  $2g$  can be found. In order to estimate  $g$ , the received preamble at  $q$ th RX antenna from  $p$ th TX antenna, corresponding to  $\mathbf{c}_{p,1}$  and  $\mathbf{c}_{p,2}$  need to be first frequency compensated by  $\hat{\theta}$  at first and then transformed into

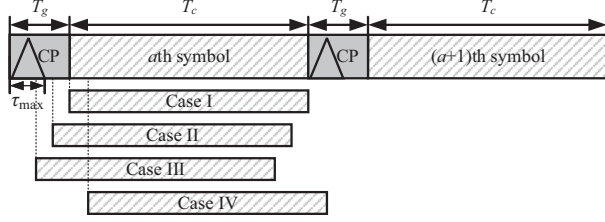


Fig. 2. Four different cases of an OFDM symbol starting point subject to STO.

the frequency domain as  $\mathbf{x}_{q,p,1}$  and  $\mathbf{x}_{q,p,2}$ , respectively. Then,  $g$  can be estimated by the difference correlation as follows:

$$\hat{g} = \arg \max_g \frac{\sum_{p=1}^{N_t} \sum_{q=1}^{N_r} \left| \sum_{k \in X_{\text{Even}}} X_{q,p,1}^* [k+2g] v_p^* [k] X_{q,p,2} [k+2g] \right|^2}{2 \sum_{p=1}^{N_t} \sum_{q=1}^{N_r} \left( \sum_{k \in X_{\text{Even}}} |X_{q,p,2} [k]|^2 \right)^2}, \quad (10)$$

where  $X_{\text{Even}}$  represents the subset of even frequency indices and  $v_p [k] = \sqrt{2} c_{p,2} [k] / c_{p,1} [k]$ ,  $k \in X_{\text{Even}}$ . Finally, the estimate can be written as

$$\hat{\varepsilon} = \frac{\hat{\theta}}{\pi} + 2\hat{g}. \quad (11)$$

#### IV. ELM-BASED RSTO AND RCFO ESTIMATION

Due to the fading channel and thermal noise, small but significant RSTO and RCFO will always exist to degrade the performance of MIMO-OFDM systems. In order to perform synchronization more accurately, the methods of ELM-based RSTO and RCFO estimations will be introduced in this section.

##### A. ELM-Based RSTO Estimation

Inspired by the idea that a neural network (NN) can learn from appropriate data, we try to further exploit (by a NN) the implicit information inside the preamble to estimate RSTO and RCFO. Compared with a DNN, an ELM only has single hidden layer and thus it has lower computational complexity, but it still has excellent performance [23]. For this reason, we choose to employ an ELM in this paper. Specifically and most importantly, we expect that the relationships between the corrupted preamble signal and synchronization offset can be “learnt” by the ELM. Therefore, it is necessary to first explain the effect of STO.

Depending on the location of the estimated starting point of an OFDM symbol, the effect of STO can vary. Fig. 2 shows four different cases of timing offset, in which the estimated starting point is perfectly accurate (**Case I**), a little early (Case II), too early (Case III), or a little late compared to exact timing (Case IV).  $T_c$ ,  $T_g$  and  $\tau_{\text{max}}$  represent the duration of the OFDM symbol, the CP and the maximum excess delay, respectively [24].

In **Case II**, the channel response to the  $(a-1)$ th OFDM symbol does not overlap with the  $a$ th OFDM symbol and so

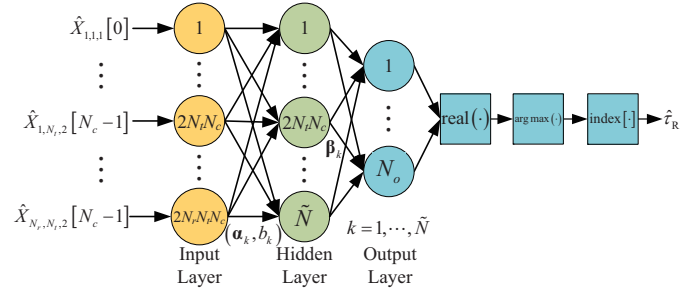


Fig. 3. The structure of an ELM-based RSTO estimator.

does not incur any ISI from the previous symbol. In this case, the received signal in the frequency domain is obtained by taking the FFT of the time domain received samples:

$$\mathbf{x}(k, a) = \mathbf{H}(k) \mathbf{s}(k, a) e^{j2\pi k\tau/N} + \mathbf{n}(k, a), \quad (12)$$

where  $\tau$  denotes the STO. Equation (12) implies that the orthogonality among subcarrier frequency components can be completely preserved. However, there exists a phase offset that is proportional to the STO  $\tau$  and subcarrier index  $k$ , forcing the signal constellation to be rotated around the origin in the complex plane.

In **Case III** and **Case IV**, the orthogonality among subcarrier components is destroyed by the ISI from the previous and the succeeding OFDM symbols, respectively. In addition, ICI will occur. A quantitative analysis of the ISI and ICI resulting from STO has been exhaustively studied in [24].

Therefore, a natural idea is that using ELM to learn the relationship between received preamble with ISI, ICI and RSTO  $\tau_R$ , where  $\tau_R = \tau - \hat{\tau}$ . Compared with DNN, ELM is considered as a general form of single layer feedforward neural networks, where the input weights and hidden layer biases of ELM are randomly generated. In other words, hidden layer outputs are always known. Hence, this structure allows the analytical calculation of the output weights during the training phase by means of least square solutions. As a result, ELM has a competitive advantage in terms of computational complexity.

The structure of a complex ELM-based RSTO estimator is illustrated in Fig. 3. The ELM-based RSTO estimator has  $2N_r N_t N_c$  input neurons,  $\tilde{N}$  hidden neurons and  $N_o$  output neurons. The input, output and weights of ELM can be fully complex.  $\hat{X}_{q,p,i} [k]$  is the input in the prediction stage, which denotes the equalized frequency domain received signal at the  $q$ th RX antenna from the  $p$ th TX antenna corresponding to  $\mathbf{c}_{p,i}$ . The data formats of the input in training and prediction stages are given in (13)-(16) and (23), respectively. The real ( $\cdot$ ) block returns the real part of the elements of the complex array and the  $\arg \max (\cdot)$  block returns the indices of the maximum values. The principle of the ELM-based RSTO estimator can be divided into two main stages: training and prediction stages.

1) *Training Stage*: In this stage, the training set  $\mathbf{N} = \{(\tilde{\mathbf{X}}_n, \mathbf{O}_n) | n = 1, \dots, N\}$  is first generated, where the  $n$ th input data of training set  $\tilde{\mathbf{X}}_n \in \mathbb{C}^{2N_r N_t N_c \times 1}$  denotes the combination vector of the preamble signal in the frequency domain by taking the FFT of the time domain received samples with corresponding RSTO. Here “index” represents an

index array including different values of RSTO. In this paper, index =  $[-N_g, \dots, N_g]$ . The target output,  $\mathbf{O}_n$  is a one-hot vector including encoded information of corresponding RSTO  $\tau_{R,n}$ . Now, for example,  $[1, 0, \dots, 0]^T$  represents  $\tau_R = -N_g$  and  $[0, \dots, 0, 1]^T$  represents  $\tau_R = N_g$ . Specifically,

$$\tilde{\mathbf{X}}_n = \text{FFT}(\text{RemoveCP}(\mathbf{X}_n)), \quad (13)$$

$$\mathbf{X}_n = \tilde{\mathbf{c}}[k] \otimes \delta[k - \tau_{R,n}], \quad (14)$$

$$\tilde{\mathbf{c}} = [\tilde{\mathbf{c}}_1^T, \dots, \tilde{\mathbf{c}}_p^T, \dots, \tilde{\mathbf{c}}_{N_t}^T]^T, \quad (15)$$

$$\tilde{\mathbf{c}}_p = \text{repmat}\left(\left[\text{CP}_{\mathbf{c}_{p,1}}^T, \mathbf{c}_{p,1}^T, \text{CP}_{\mathbf{c}_{p,2}}^T, \mathbf{c}_{p,2}^T\right]^T, N_r, 1\right). \quad (16)$$

and

$$\tau_{R,n} = \text{index} \left[ \begin{array}{c} \arg \max (o_i) \\ 1 \leq i \leq 2N_g+1 \end{array} \right], \quad (17)$$

where  $\mathbf{O}_n = [o_1, o_2, \dots, o_{2N_g+1}]^T$ . In Equation (13), the pseudo-function ‘‘RemoveCP’’ and ‘‘FFT’’ represent respectively removing all the CPs and taking the  $N_c$ -point fast Fourier transform. Note that, in Equation (14),  $\delta[k - \tau_{R,n}]$  denotes a delayed Kronecker delta function. The absent elements of  $\tilde{\mathbf{c}}$  will be filled by zero padding.

In step1 of Algorithm 1 (see later), the complex input weight  $\alpha_k$  and complex bias  $b_k$  (see also Fig.3) are generated from the uniform distribution  $U(-0.1, 0.1)$ , where  $\alpha_k \in \mathbb{C}^{2N_r N_t N_c \times 1}$  is the input weight vector connecting input neurons to the  $k$ th hidden neuron and  $\alpha = [\alpha_1, \dots, \alpha_k, \dots, \alpha_{\tilde{N}}]$  and  $\mathbf{b} = [b_1, \dots, b_k, \dots, b_{\tilde{N}}]$ . Once the input weights and biases are chosen, the output of the hidden layer can be given by

$$\mathbf{D}_{\text{Training}} = g_c(\alpha^T \tilde{\mathbf{X}} + \mathbf{b}) \quad (18)$$

where  $\tilde{\mathbf{X}} = [\tilde{\mathbf{X}}_1 \ \tilde{\mathbf{X}}_2 \ \dots \ \tilde{\mathbf{X}}_N] \in \mathbb{C}^{2N_r N_t N_c \times N}$ .

We expect that the output of the ELM could be close to the target output  $\mathbf{O}$ , so

$$\beta \mathbf{D}_{\text{Training}} = \mathbf{O}. \quad (19)$$

Generally,  $\beta = [\beta_1, \dots, \beta_k, \dots, \beta_{\tilde{N}}] \in \mathbb{C}^{N_o \times \tilde{N}}$  and  $\beta_k = [\beta_{k1}, \beta_{k2}, \dots, \beta_{kN_o}]^T \in \mathbb{C}^{N_o \times 1}$ , where  $\beta_k$  denotes the output weight vector connecting the  $k$ th hidden neuron and the output neurons and  $N_o$  denotes the number of output neurons. For the ELM-based RSTO estimator,  $N_o = 2N_g + 1$ . Under the criterion of minimizing the squared errors, the least squares (LS) solution is given by

$$\hat{\beta} = \min_{\beta} \|\beta \mathbf{D}_{\text{Training}} - \mathbf{O}\| = \mathbf{O} \mathbf{D}_{\text{Training}}^\dagger. \quad (20)$$

The training algorithm for an ELM-based RSTO estimator can be summarized as follows:

---

### Algorithm 1 The Training Algorithm for an ELM-based RSTO Estimator

---

We are given a training set  $\mathbf{N} = \{(\tilde{\mathbf{X}}_n, \mathbf{O}_n) | n = 1, \dots, N\}$ , complex activation function  $g_c(\cdot)$ , and hidden neuron number  $\tilde{N}$ .  $\tilde{\mathbf{X}}_n \in \mathbb{C}^{2N_r N_t N_c \times 1}$ ,  $\mathbf{O}_n$  is a one-hot vector and these two correspond to the input and desired output of the ELM, respectively.

**Step 1:** Randomly choose the values of complex input weight  $\alpha_k$  and the complex bias  $b_k$ ,  $k = 1, \dots, \tilde{N}$ .

**Step 2:** Calculate the complex hidden layer output matrix  $\mathbf{D}_{\text{Training}}$ .

**Step 3:** Calculate the complex output weight  $\beta$  using  $\hat{\beta} = \mathbf{O} \mathbf{D}_{\text{Training}}^\dagger$ , where  $\mathbf{O} \in \mathbb{C}^{N_o \times N}$ .

---

2) *Prediction Stage:* For an ELM-based RSTO estimator, we assume that LS channel estimation is used or the perfect CSI is known. Thus the equalized preamble can be given by<sup>1</sup>

$$\hat{X}_{q,p,i}[k] = X_{q,p,i}[k] / \mathbf{H}_{q,p,i}[k]. \quad (21)$$

The output of hidden layer can be calculated as

$$\mathbf{D}_{\text{Prediction}} = g_c(\alpha^T \hat{\mathbf{x}} + \mathbf{b}) \quad (22)$$

where

$$\hat{\mathbf{x}} = \left[ \hat{\mathbf{x}}_{1,1,1}^T, \hat{\mathbf{x}}_{1,1,2}^T, \dots, \hat{\mathbf{x}}_{N_t, N_r-1,1}^T, \hat{\mathbf{x}}_{N_t, N_r-1,2}^T, \hat{\mathbf{x}}_{N_t, N_r,1}^T, \hat{\mathbf{x}}_{N_t, N_r,2}^T \right]^T. \quad (23)$$

Note that the input, output and all the weights and biases of ELM in this paper are complex values but RSTO and RCFO are real values. Therefore, the operator  $\text{real}(\cdot)$  following the output of ELM is necessary. By expressing  $\text{real}(\hat{\beta} \mathbf{D}_{\text{Prediction}})$  as  $\text{real}(\hat{\beta} \mathbf{D}_{\text{Prediction}}) = [\hat{o}_1, \hat{o}_2, \dots, \hat{o}_{2N_g+1}]^T$ , the RSTO is given as

$$\hat{\tau}_R = \text{index} \left[ \begin{array}{c} \arg \max (\hat{o}_i) \\ 1 \leq i \leq 2N_g+1 \end{array} \right]. \quad (24)$$

### B. ELM-Based RCFO Estimation

As Fig. 4 illustrates, the ELM-based RCFO estimator has  $2N_r N_t N_c$  input neurons,  $\tilde{N}$  hidden neurons and only one output neuron. Here, we use  $\varepsilon_R$  to denote the RCFO, where  $\varepsilon_R = \varepsilon - \hat{\varepsilon}$ .

1) *Training Stage:* Before ELM can be deployed to estimate RCFO, it has to learn the prior knowledge from the training set. The training algorithm for an ELM-based RCFO estimator can be summarized as follows:

<sup>1</sup>A minimum mean-square error (MMSE) channel estimator cannot be deployed before the STO is estimated because the STO can degrade the performance of the MMSE channel estimator [25]. However, the simulation results in Section V still include the ELM-based STO estimator with MMSE channel estimation. The introduction of the MMSE channel estimator is given in the next subsection.

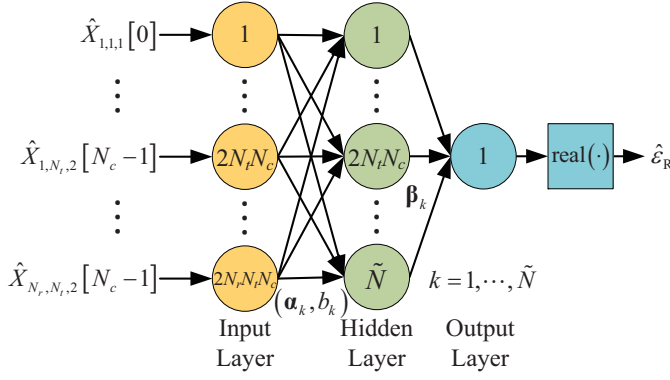


Fig. 4. The structure of an ELM-based RCFO estimator.

---

**Algorithm 2** The Training Algorithm for an ELM-based RCFO Estimator
 

---

We are given a training set  $\mathbf{N} = \{(\tilde{\mathbf{I}}_n, O_n) | n = 1, \dots, N\}$ , complex activation function  $g_c(\cdot)$ , and hidden neuron number  $\tilde{N}$ .  $\tilde{\mathbf{I}}_n \in \mathbb{C}^{2N_r N_t N_c \times 1}$ ,  $O_n$  is a real number and these two correspond to the input and desired output of the ELM, respectively. Here,  $O_n$  denotes a given RCFO.

**Steps 1, 2 and 3:** Refer to **Algorithm 1**.

---

Specifically, the  $n$ th input data of training set  $\tilde{\mathbf{I}}_n$  denotes the preamble with corresponding RCFO,  $\varepsilon_R = O_n$ , where

$$\tilde{\mathbf{I}}_n = \text{FFT}(\text{RemoveCP}(\mathbf{I}_n)), \quad (25)$$

$$\mathbf{I}_n = [\tilde{\mathbf{c}}_1^T, \dots, \tilde{\mathbf{c}}_p^T, \dots, \tilde{\mathbf{c}}_{N_t}^T]^T \odot [\tilde{\mathbf{o}}_1^T, \dots, \tilde{\mathbf{o}}_p^T, \dots, \tilde{\mathbf{o}}_{N_t}^T]^T, \quad (26)$$

$$\tilde{\mathbf{c}}_p = \text{repmat}\left(\left[\text{CP}_{\mathbf{c}_{p,1}}^T, \mathbf{c}_{p,1}^T, \text{CP}_{\mathbf{c}_{p,2}}^T, \mathbf{c}_{p,2}^T\right]^T, N_r, 1\right), \quad (27)$$

$$\tilde{\mathbf{o}}_p = \text{repmat}(\mathbf{o}_p, N_r, 1), \quad (28)$$

and

$$\mathbf{o}_p = \begin{bmatrix} e^{2\pi j[1+2(p-1)(N_c+N_g)]O_n/N_c} \\ \vdots \\ e^{2\pi j[2(N_c+N_g)+2(p-1)(N_c+N_g)]O_n/N_c} \end{bmatrix}. \quad (29)$$

In **step1** of **Algorithm 2**, the generation of the input weight  $\alpha_k$  and bias  $b_k$  are the same as **step1** in **Algorithm 1**. The output of the hidden layer can be given by

$$\mathbf{D}_{\text{Training}} = g_c(\alpha^T \tilde{\mathbf{I}} + \mathbf{b}) \quad (30)$$

where  $\tilde{\mathbf{I}} = [\tilde{\mathbf{I}}_1 \quad \tilde{\mathbf{I}}_2 \quad \dots \quad \tilde{\mathbf{I}}_N] \in \mathbb{C}^{2N_r N_t N_c \times N}$ .

We would expect that the output of the ELM could be close to the target output  $\mathbf{O}$ , so  $\beta \mathbf{D}_{\text{Training}} = \mathbf{O}$ . For the ELM-based RCFO estimator,  $N_o = 1$ . The LS solution is then given by

$$\hat{\beta} = \mathbf{O} \mathbf{D}_{\text{Training}}^\dagger. \quad (31)$$

2) *Prediction (Estimation) Stage:* Since the received preambles have been corrupted by the fading channel, channel estimation and equalization need to be carried out. Now that  $\mathbf{c}_{p,2}$  is known and fully occupies the subcarriers, the minimum mean-square error (MMSE) estimate of frequency impulse response [25] from the  $p$ th TX antenna to the  $q$ th RX antenna is given by

$$[\hat{\mathbf{H}}_{q,p}[0], \dots, \hat{\mathbf{H}}_{q,p}[N_c-1]]^T = \mathbf{F} \mathbf{Q}_{\text{MMSE}} \mathbf{F}^H \mathbf{c}_{q,p,2}^H \mathbf{x}_{q,p,2}, \quad (32)$$

where  $\mathbf{Q}_{\text{MMSE}}$  can be shown to be

$$\mathbf{Q}_{\text{MMSE}} = \mathbf{R}_{\text{gg}} \left[ \left( \mathbf{F}^H \mathbf{c}_{q,p,2}^H \mathbf{c}_{q,p,2} \mathbf{F} \right)^{-1} \sigma_n^2 + \mathbf{R}_{\text{gg}} \right]^{-1} \times \left( \mathbf{F}^H \mathbf{c}_{q,p,2}^H \mathbf{c}_{q,p,2} \mathbf{F} \right)^{-1}. \quad (33)$$

$\mathbf{R}_{\text{gg}}$  is the auto-covariance matrix of  $[g_{q,p}(0), \dots, g_{q,p}(L-1)]^T$  for any  $(q, p)$ . In other words, all the auto-covariance matrices of subchannels are the same.  $\sigma_n^2$  denotes the noise variance  $\text{E}\{|n_k^2|\}$ . Here, we assume that the auto-covariance matrices of all the subchannels between the TX antennas and the RX antennas are the same, so the subscripts of  $\mathbf{R}_{\text{gg}}$  are omitted. Then, the equalized preamble can be given by

$$\hat{X}_{q,p,i}[k] = X_{q,p,i}[k] / \hat{\mathbf{H}}_{q,p,i}[k]. \quad (34)$$

The calculation of the output of the hidden layer and  $\hat{\mathbf{x}}$  are same as Equation (22) and (23), respectively. Finally, the RCFO is estimated as

$$\hat{\varepsilon}_R = \text{real}(\hat{\beta} \mathbf{D}_{\text{Prediction}}). \quad (35)$$

### C. How Do We Deal with the ‘‘Chicken or the Egg’’ Causality Dilemma?

Most of the existing machine learning-based physical techniques require labeled data with perfect CSI in the training stage. The question raised in these studies was that it is impossible to acquire (estimate) the perfect CSI in real channel scenarios due to the existence of thermal noise. In other words, which came first: the labeled data or the perfect CSI? The essential reason for this dilemma is that CSI is random and therefore it cannot be estimated or predicted perfectly. Besides, the computational cost to learn the relationship between random variables and target output is extremely high. Nevertheless, can we deal with this causality dilemma?

In this paper, we generate training data by letting preamble to be corrupted by RSTO and RCFO without the effects of multipath fading channel and thermal noise. There are two main purposes for this. The first aims to make ELM learn the relationship between the corrupted preamble and its corresponding RSTO and RCFO. The second purpose is to avoid the ‘‘chicken and the egg’’ causality dilemma. However, it should be noticed that the input of the ELM in the prediction stage is the preamble corrupted by RSTO, RCFO, multipath fading channel and thermal noise. Therefore, the only question is whether the purpose method can outperform traditional method. The following section will provide exhaustive simulation results and comparisons.

## V. SIMULATION RESULTS AND COMPARISONS

### A. Simulation Setup

In this section, the performance of the proposed ELM-based RSTO and RCFO estimators is demonstrated. In order to avoid the occurrence of the **Case IV** in Fig. 2, the timing point will be set  $N_g/4$  points ahead of the estimated value from the traditional estimator in the case of a fading channel.<sup>2</sup> For the estimation of CFO, the performance of the estimator based on the traditional method and its Cramér-Rao lower bound (CRLB) will also be studied and used as a benchmark. Note that the CRLB is equal to the variance of traditional CFO estimator [4]

$$\text{var}(\hat{\varepsilon} - \varepsilon) = \frac{1}{\pi^2 N_t N_r V \rho} \quad (36)$$

where  $V$  is the length of identical halves in the first part of the preamble and  $\rho = (P/N_t) \sigma_n^2$  denotes the SNR per receive antenna when the preamble is transmitting and  $P$  is the total transmit power.<sup>3</sup> Note that (36) is approximately accurate under the condition of small errors ( $\hat{\varepsilon} - \varepsilon$ ) and high SNR and it is derived in the appendix. We assume that timing synchronization is perfect ( $\hat{\tau} = \tau$ ) when the performance of both the traditional and the ELM-based CFO estimators are evaluated. For the numerical simulations, we set  $N_c = 64$ ,  $N_g = N_c/4$  and sampling frequency  $f_s = 4 \times 10^6$ . The wireless fading channel is modeled as an exponential model and quasistatic assumption is guaranteed during each OFDM symbol. The activation function  $g_c$  is  $\text{arcsinh}(z) = \int_0^z dt / \left[ (1+t^2)^{1/2} \right]$  [26], where  $z \in \mathbb{C}$ . Note that, for a fair comparison, we keep the total transmitting power the same as in the single-input single-output (SISO) case. Therefore, the power per TX antenna is scaled down by a factor  $N_t$ .

For an exponentially decaying PDP, the root mean square (RMS) delay spread  $\tau_{\text{RMS}} = 2 \times 10^{-6}$ s, and the coherence bandwidth  $B_c = 1/\tau_{\text{RMS}} = 5 \times 10^5$ Hz. The PDP is given by

$$P_l = \exp\left(\frac{-2\pi B_c \tau_l}{\sqrt{3}}\right) \quad (37)$$

where the delay of  $l$ th path is set as  $\tau_l = lT_s$  and  $L = 8$ .

### B. The Performance of the ELM-based RSTO Estimator

As it is instructive to observe the bias as well as the MSE of an estimator (where  $\text{MSE} = \text{variance} + (\text{bias})^2$ ), we will examine both the bias and the MSE of the proposed estimator and compare this with the traditional estimator.

In Fig. 5, the bias of the STO estimation is demonstrated as a function of the average SNR per receive antenna, where  $\tilde{N} = 2^{14}$ . The results from Monte Carlo simulations averaged over  $3 \times 10^5$  channel realizations are shown. In the case of both an AWGN channel and a frequency-selective fading channel with perfect CSI information, it can be seen that the proposed ELM-based estimator has a much smaller bias than the traditional

<sup>2</sup>In order to avoid ISI, the FFT window start position has to be put in advance of the estimated point obtained by the coarse STO estimation algorithm [12].

<sup>3</sup>(36) also can be written as  $\text{var}(\hat{\varepsilon} - \varepsilon) = \frac{1}{\pi^2 N_t N_r V \rho'}$  where the SNR per receive antenna is defined as  $\rho' = P \sigma_n^2$ .

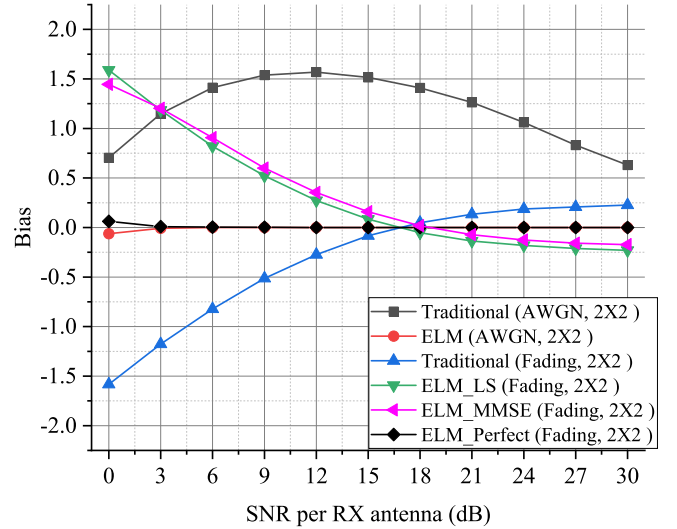


Fig. 5. Bias performance comparison between the traditional STO estimator and the proposed ELM-based STO estimator for a 2x2 system with a multipath fading channel.

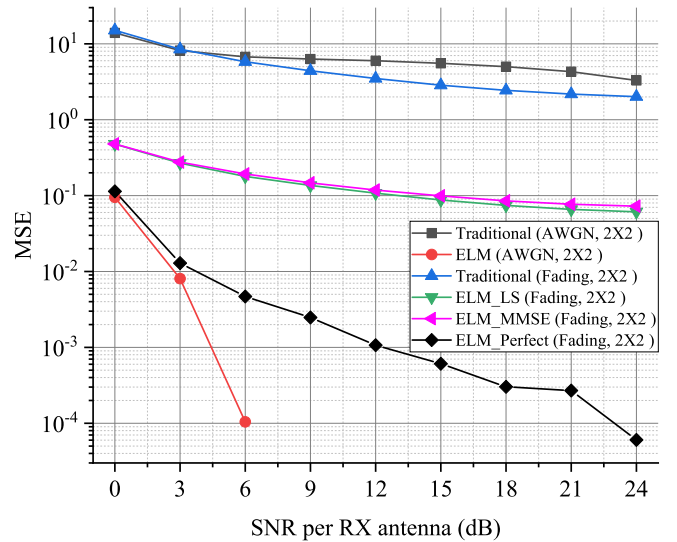


Fig. 6. MSE performance comparison between the traditional STO estimator and the proposed ELM-based STO estimator for a 2x2 system with a multipath fading channel.

estimator. In the cases of a frequency-selective fading channel with LS and MMSE channel estimation, the ELM-based STO estimator does not show a gain in terms of bias.

Fortunately, without perfect knowledge about the fading channel, the ELM-based STO estimator still achieve a gain compared with the traditional STO estimator in terms of MSE. In Fig. 6, the MSE of the STO estimation is demonstrated as a function of the average SNR per receive antenna, where  $\tilde{N} = 2^{14}$ . Even if the ELM-based estimator acquires the imperfect CSI just by using a LS or an MMSE channel estimate, the ELM-based STO estimator shows significant gains compared with the traditional STO estimator.

TABLE I  
TRAINING SETS FOR DIFFERENT MIMO SYSTEMS

MIMO System	Range of RCFO	Interval of RCFO
1X1	$[-0.0025, 0.0025]$	$5.0 \times 10^{-6}$
2X2	$[-0.0025, 0.0025]$	$2.5 \times 10^{-6}$
3X3 (Fading Channel)	$[-0.0030, 0.0030]$	$5.0 \times 10^{-6}$
3X3 (AWGN Channel)	$[-0.05, 0.05]$	$1.0 \times 10^{-4}$

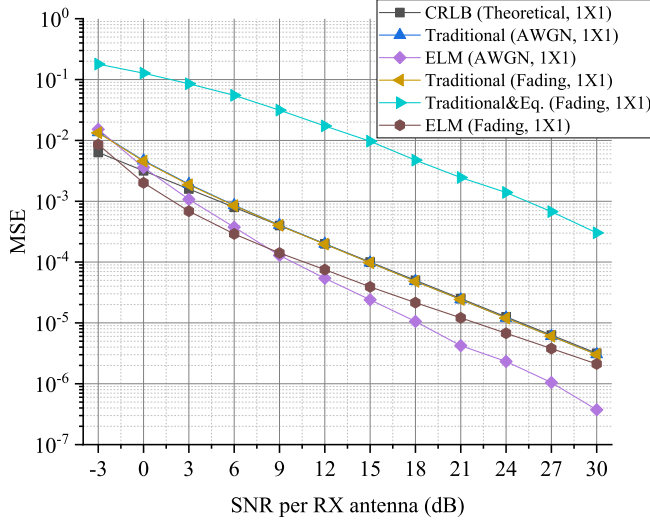


Fig. 7. MSE performance comparison between the traditional CFO estimator and the proposed ELM-based CFO estimator for a  $1 \times 1$  system from theory and simulations with AWGN and a multipath fading channel ( $\varepsilon = -0.05$ ,  $O_n \in \{5.0 \times 10^{-6}k | k = -500, \dots, 500\}$  and  $\tilde{N} = 2^{11}$ ).

### C. Performance of the ELM-based RCFO Estimator

The performance of a NN depends on the training set. Specifically, for an ELM-based RCFO estimator, the range and interval of the desired output in a training set should be chosen carefully. In this paper, the training sets for different MIMO systems are summarized in Table I.

1) *MSE Performance*: In Fig. 7, the MSE of the CFO estimation is demonstrated as a function of the average SNR per receive antenna, where  $\tilde{N} = 2^{11}$ . The theoretical value from (36) is shown together with results from Monte Carlo simulations averaged over  $10^5$  channel realizations. As seen from Fig. 7, the MSE curve of the traditional method almost perfectly overlaps that of the CRLB. The theoretical value is a good estimate of the MSE for high SNR values but underestimates the MSE compared with simulation results for low SNR. Note that the CRLB expresses a lower bound on the variance of unbiased estimators of a deterministic parameter. A biased approach can result in both a variance and a MSE that are below the unbiased CRLB. Specifically, in the case of AWGN, when SNR = -3dB, ELM obtains a slightly larger MSE value compared with simulation results for the traditional method. Fortunately, we can see that the performance improvement between ELM and the traditional method increases with SNR, and when SNR = 21dB ELM achieves an SNR gain of about 9dB over the traditional method at a MSE value of  $4.22 \times 10^{-6}$ .

This can be explained by the fact that the ELM can reuse

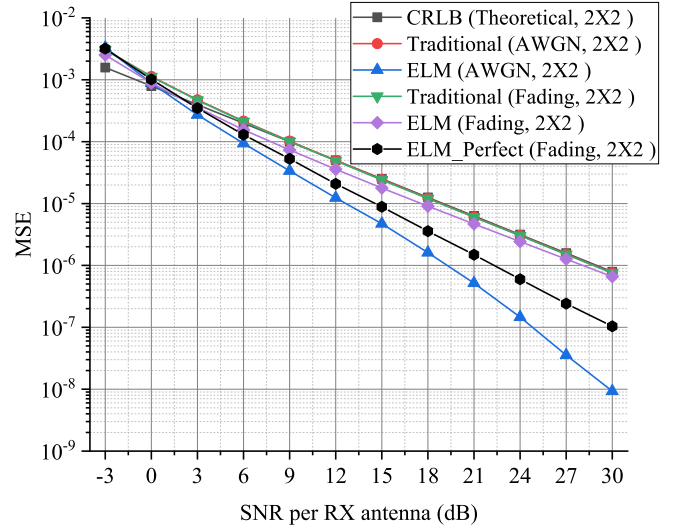


Fig. 8. MSE performance comparison between the traditional CFO estimator and the proposed ELM-based CFO estimators for a  $2 \times 2$  system from theory and simulations with AWGN and a multipath fading channel ( $\varepsilon = -0.05$ ,  $O_n \in \{2.5 \times 10^{-6}k | k = -1000, \dots, 1000\}$  and  $\tilde{N} = 2^{14}$ ).

the preamble exhaustively and also the mapping relationships between RCFOs and their corresponding preambles with RCFOs. In the case of a frequency-selective fading channel, the largest SNR gain over a traditional method, about 4.5dB, is achieved when SNR = 6dB. This kind of the gain becomes insignificant when SNR > 27dB. Besides, in order to prove that the gain of ELM is not just a result of channel estimation and equalization, the curve of “Traditional&Eq.” shows the MSE performance of the traditional method with channel estimation and equalization. Specifically, the method “Traditional&Eq.” performs traditional CFO estimation twice. The first CFO estimation uses the traditional method. Then, channel estimation and equalization are performed by using the frequency corrected preamble signal. Finally, the traditional CFO estimation method is performed again to estimate RCFO by using the frequency corrected and equalized preamble signal. It can be seen that its performance seriously degrades, which means that channel estimation and equalization cannot enhance the performance of the traditional CFO estimator.

Fig. 8 presents the MSE curves of the traditional and proposed ELM-based CFO estimators for a  $2 \times 2$  system, where  $\tilde{N} = 2^{14}$ . Similar to the observations in Fig. 7, in the case of an AWGN channel, the MSE performance of the ELM still outperforms that of the traditional method. Using the ELM, when SNR = 18dB, about 9dB SNR gain over traditional method is achieved at MSE =  $2.16 \times 10^{-6}$ . In the case of a frequency-selective fading channel, by comparing Fig. 8 with Fig. 7, we find that the gains of ELM over the traditional method for a  $2 \times 2$  system (about 1.5dB) are lower than that for  $1 \times 1$  system (about 1.5-4.5dB). We conjecture that this is because the accuracy of channel estimation limits the CFO estimation performance of the ELM.

In order to prove this conjecture, we also perform the simulation for the ELM estimator with perfect channel state information (CSI). In Fig. 8, the curve “Perfect-ELM” illus-

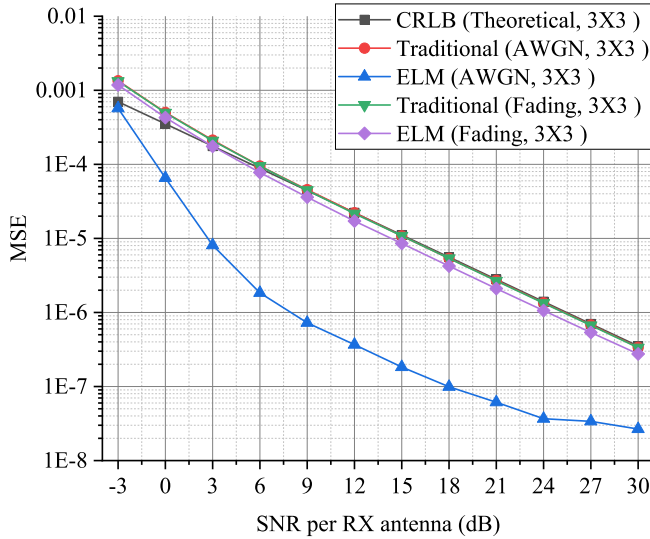


Fig. 9. MSE performance comparison between the traditional CFO estimator and the proposed ELM-based CFO estimator for a  $3 \times 3$  system from theory and simulations with AWGN and a multipath fading channel ( $\varepsilon = -0.05$ ,  $\tilde{N} = 2^{17}$  and AWGN:  $O_n \in \{1.0 \times 10^{-4}k | k = -500, \dots, 500\}$ ; Fading:  $O_n \in \{5.0 \times 10^{-6}k | k = -600, \dots, 600\}$ ).

trates the performance of the ELM with perfect CSI. It can be seen that, under the condition of knowing perfect CSI, the MSE performance of the ELM under the condition of fading is closer to that under the condition of AWGN compared to that of ELM without perfect CSI. The gain from perfect CSI increases with the increase of SNR. So we can conjecture that the performance of the ELM-based scheme is highly dependent on the accuracy of the CSI.

Fig. 9 presents the MSE curves of the traditional and the proposed ELM-based CFO estimators for a  $3 \times 3$  MIMO system, where  $\tilde{N} = 2^{17}$ . Note that for a  $3 \times 3$  system, the ELM is trained by different training sets separately in order to achieve the best performance under AWGN and fading channel conditions. In the case of an AWGN channel, when  $\text{SNR} = -3\text{dB}$ , the MSE performance of the ELM is slightly better than the CRLB but its MSE decreases rapidly with an increase of SNR. When  $\text{SNR} = 12\text{dB}$ , about 18dB SNR gain over the traditional method is achieved by the ELM-based method. By comparing Fig. 9 with Fig. 8 and Fig. 7, the gain of the ELM-based method over the traditional method increases with the increase in the number of RX antennas. This is because the MSE performance of the ELM relates to the number of the receive antennas. When  $\text{SNR} \geq 21\text{dB}$ , the gains are not as high as the highest gains. The reason is that the gain of ELM is from both noise suppression and mining information exhaustively from preambles. In the case of a frequency-selective fading channel, the ELM can obtain about 1.5dB gain of MSE when  $\text{SNR} \geq 3\text{dB}$ , which is similar with the case for a  $2 \times 2$  system.

2) *Robustness Analysis*: In this section, we analyse the robustness of the proposed ELM scheme. Fig. 10 shows the MSE of ELM under various RCFOs when  $\text{SNR} = 15\text{dB}$  and  $30\text{dB}$ . It can be seen that the MSE increases with an increase of RCFO. By comparing Fig. 10 with Fig. 8, when  $\text{SNR} = 30\text{dB}$

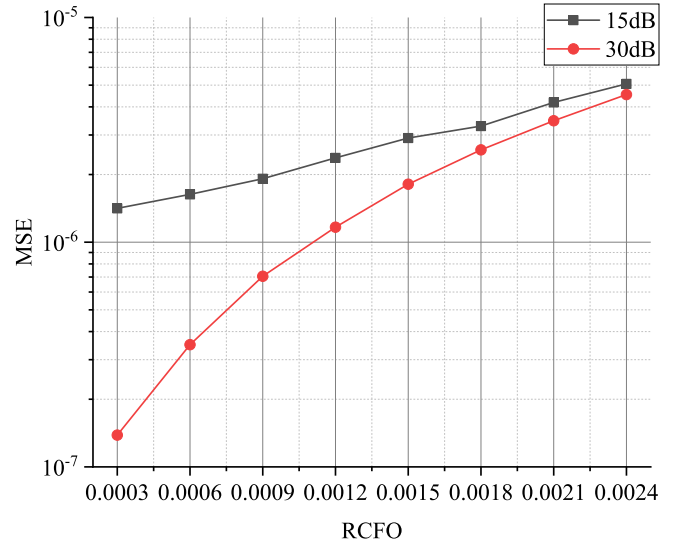


Fig. 10. MSE versus RCFO curves of the proposed ELM-based CFO estimator for a  $2 \times 2$  system ( $O_n \in \{2.5 \times 10^{-6}k | k = -1000, \dots, 1000\}$  and  $\tilde{N} = 2^{14}$ ).

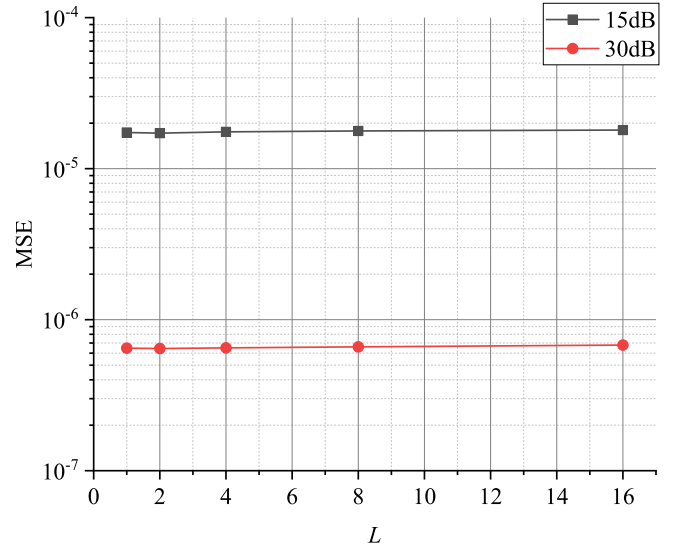


Fig. 11. MSE versus the number of paths of a fading channel ( $L$ ) of the proposed ELM-based CFO estimator for a  $2 \times 2$  system ( $O_n \in \{2.5 \times 10^{-6}k | k = -1000, \dots, 1000\}$  and  $\tilde{N} = 2^{14}$ ).

and  $\text{RCFO} \geq 0.0012$ , the MSE of the ELM is higher than that in Fig. 8 ( $\text{MSE} > 10^{-6}$ ). However, when  $\text{SNR} = 15\text{dB}$  and  $\text{RCFO} \leq 0.0024$ , the MSE of ELM is lower than that in Fig. 8 ( $\text{MSE} < 10^{-5}$ ). This can be explained by the fact that the performance advantage and robustness of the ELM-based method are more significant in medium SNR.

Fig. 11 shows the MSE of the ELM under a different number of channel paths when  $\text{SNR} = 15\text{dB}$  and  $30\text{dB}$ . It can be seen that, with increase of  $L$ , the MSE of the ELM increases slightly, which means that the proposed method is robust enough to handle frequency-selective fading channels with different numbers of paths.

3) *Generalization Error Analysis*: Generalization is a term used to describe the ability of a model to react to new

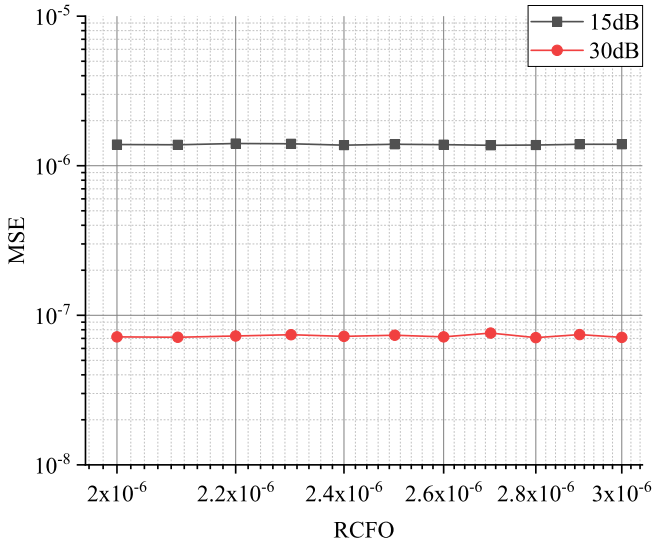


Fig. 12. MSE versus the RCFO not belonging to a training set of the proposed ELM-based CFO estimator for a  $2 \times 2$  system ( $O_n \in \{2.5 \times 10^{-6}k | k = -1000, \dots, 1000\}$  and  $\tilde{N} = 2^{14}$ ).

data. That is, after being trained on a training set, can a model “digest” new data and make accurate predictions? In this paper, we also use MSE to evaluate the generalization ability of the ELM. Specifically, an RCFO not belonging to the training set is used to verify the generalization of a trained ELM-based RCFO estimator. The generalization ability of ELM can be analyzed according to Fig. 12, where we have used RCFOs that do not belong to the training set  $O_n \in \{2.5 \times 10^{-6}k | k = -1000, \dots, 1000\}$ . By comparing Fig. 12 with Fig. 8, the performance of the ELM-based RCFO estimator does not change significantly when it handles those unfamiliar RCFOs. It can be concluded that the ELM-based RCFO estimator shows excellent generalization when it processes an RCFO not belonging to the training set.

#### D. Complexity Analysis

We use the number of complex multiplications (CMs) to measure the computational complexity. For simplicity, the numbers of CMs for calculating the Moore-Penrose generalized matrix inverse of a  $I \times O$  matrix is denoted as  $C_{\text{pinv}} (OI^2)$ . We compare the proposed complex ELM-based method with DNN-based method. We assume that the input dimension and output dimension of the complex ELM-based method are  $I$  and  $O$ , respectively. For DNN-based method, we split a complex number into a real part and an imaginary part. Thus, the input dimension and the output dimension of DNN-based method are  $2I$  and  $2O$ , respectively. In DNN-based method, there are real-valued multiplications. When calculating the computational complexity, we consider that four real-valued multiplications are equivalent to one CM.

The machine learning-based method has two phases, i.e., the training phase and the prediction phase, and we analyse the computational complexity for the two phases individually.

As for the training phase, the calculation of the output weights of complex ELM-based method requires  $C_{\text{pinv}} (N\tilde{N}^2) +$

$N (\tilde{N} + O)$  CMs where  $\tilde{N}$  is the number of hidden neurons in the complex ELM and  $N$  is the number of the training samples. The training complexity of DNN-based method is difficult to derive using the number of CMs because it is trained iteratively with forward propagation (FP) and backpropagation (BP). Generally, the training complexity of DNN is obviously higher than complex ELM, and this results that the time consumption of training is hard to satisfy the latency constraint in practical uses.

As for the prediction phase, the required numbers of CMs of complex ELM and DNN are  $IO\tilde{N}$  and  $IO \sum_{l=1}^{N_l} n_l n_{l-1}$ , respectively.  $N_l$  and  $n_l$  denotes the number of hidden layers and the number of neurons at the  $l$ th hidden layer, respectively. It can be seen that the prediction complexity of DNN is high than the complex ELM.

## VI. CONCLUSIONS AND FUTURE WORK

In this paper, we have proposed an ELM-based fine timing and frequency synchronization scheme in order to improve the performance of existing estimators. The proposed scheme does not require additional preamble and the training processes can be carried out fully offline without any prior information about the channels. Simulation results have shown that the proposed ELM-based synchronization scheme outperforms or achieves comparable performance in terms of MSE with existing traditional synchronization algorithms. In addition, the proposed scheme shows robustness under various channels with different parameters and a generalization ability towards any RCFO outside the training set.

The simulation results have shown that the performance of ELM-based scheme relates to the accuracy of the CSI. Besides, it should be noticed that channel equalization can neutralize the effects of both STO and fading channel. Therefore, this makes it difficult to obtain the received preamble signal affected by just the STO alone. In other words, the accurate CSI is still indispensable for the deployment of machine learning in communications systems. Therefore, incorporating ELM into transmitter design, synchronization and channel estimation and equalization jointly within system design is a promising future research direction.

### APPENDIX A

#### VARIANCE OF THE CFO ESTIMATION FOR A MIMO SYSTEM UNDER AWGN CHANNEL (SEE (36))

We use the method in [2] and [27] to derive the variance of the CFO estimate for a MIMO system. According to (8), for a given  $\epsilon$ , subtract the corresponding phase,  $2\pi\epsilon$ , from each product to obtain the tangent of the phase error

$$\tan [\pi (\hat{\epsilon} - \epsilon)] = \frac{\sum_{p=1}^{N_t} \sum_{q=1}^{N_r} \sum_{i=d_p-(V-1)}^{d_p} \text{Im} [r_q^* (i-V) r_q (i) e^{-2\pi j \epsilon}]}{\sum_{p=1}^{N_t} \sum_{q=1}^{N_r} \sum_{i=d_p-(V-1)}^{d_p} \text{Re} [r_q^* (i-V) r_q (i) e^{-2\pi j \epsilon}]} \quad (38)$$

where  $d_p = d - (N_t - p) N_{\text{train}}$ ,  $V$  denotes the length of identical halves in the first part of the preamble and  $r_q (i) = \tilde{r}_q (i) + n_q (i)$ .  $n_q (i)$  denotes the time domain noise of  $i$ th

sample of the received signal on the  $q$ th antenna. For  $|\hat{\varepsilon} - \varepsilon| \ll 1/\pi$ , the tangent can be approximated by its argument so that

$$\hat{\varepsilon} - \varepsilon \approx \frac{\sum_{p=1}^{N_t} \sum_{q=1}^{N_r} \sum_{i=d_p-(V-1)}^{d_p} \text{Im}\{[\tilde{r}_q(i-V)+n_q(i)]e^{-2\pi j\varepsilon}\}[\tilde{r}_q^*(i)+n_q(i)]e^{-2\pi j\varepsilon}\}}{\pi \sum_{p=1}^{N_t} \sum_{q=1}^{N_r} \sum_{i=d_p-(V-1)}^{d_p} \text{Re}\{[\tilde{r}_q(i-V)+n_q(i)]e^{-2\pi j\varepsilon}\}[\tilde{r}_q^*(i)+n_q(i)]e^{-2\pi j\varepsilon}\}}. \quad (39)$$

According to the method in [2], at high SNR, a condition compatible with successful communications signalling means that (39) may be approximated by

$$\hat{\varepsilon} - \varepsilon \approx \frac{\left\{ \sum_{p=1}^{N_t} \sum_{q=1}^{N_r} \sum_{i=d_p-(V-1)}^{d_p} \text{Im}[n_q(i)\tilde{r}_q^*(i-V)e^{-2\pi j\varepsilon} + \tilde{r}_q(i-V)n_q^*(i-V)] \right\}}{\left\{ \pi \sum_{p=1}^{N_t} \sum_{q=1}^{N_r} \sum_{i=d_p-(V-1)}^{d_p} |\tilde{r}_q(i)|^2 \right\}}. \quad (40)$$

It is easy to show that

$$E[\hat{\varepsilon} - \varepsilon | \varepsilon, \{\tilde{r}_q\}] = 0. \quad (41)$$

Therefore, for small errors, the estimate is conditionally unbiased. Then, the conditional variance of the estimate is easily determined for (40) as

$$\text{Var}[\hat{\varepsilon} | \varepsilon, \{\tilde{r}_q\}] = \frac{1}{\pi^2 N_t N_r V \rho}. \quad (42)$$

Finally, note that in this paper,  $\rho = \sigma_{\tilde{r}_q}^2 / \sigma_n^2 = (P/N_t) \sigma_n^2$  denotes the SNR per receive antenna when the preamble is transmitting and  $P$  is the total transmit power.

#### ACKNOWLEDGEMENT

The authors would like to acknowledge the help received from Longguang Wang. In addition, Jun Liu gratefully acknowledges the financial support received from the China Scholarship Council (CSC) and the School of Electronic and Electrical Engineering, University of Leeds, UK. He also wants to thank, in particular, the inspiration and care received from Yanling (Julia) Zhu during the period of this COVID-19 pandemic.

#### REFERENCES

- [1] N. Rajatheva, I. Atzeni, E. Bjornson, and et al., "White paper on broadband connectivity in 6G," *arXiv preprint arXiv:2004.14247*, 2020.
- [2] P. H. Moose, "A technique for orthogonal frequency division multiplexing frequency offset correction," *IEEE Transactions on Communications*, vol. 42, no. 10, pp. 2908–2914, 1994.
- [3] T. M. Schmidl and D. C. Cox, "Robust frequency and timing synchronization for OFDM," *IEEE Transactions on Communications*, vol. 45, no. 12, pp. 1613–1621, 1997.
- [4] A. van Zelst and T. C. W. Schenk, "Implementation of a MIMO OFDM-based wireless LAN system," *IEEE Transactions on Signal Processing*, vol. 52, no. 2, pp. 483–494, 2004.
- [5] A. N. Mody and G. L. Stuber, "Synchronization for MIMO OFDM systems," in *GLOBECOM'01. IEEE Global Telecommunications Conference (Cat. No. 01CH37270)*, vol. 1, 2001, pp. 509–513 vol.1.
- [6] M. Ghogho and A. Swami, "Training design for multipath channel and frequency-offset estimation in MIMO systems," *IEEE Transactions on Signal Processing*, vol. 54, no. 10, pp. 3957–3965, 2006.
- [7] P. Cheng, Z. Chen, F. de Hoog, and C. K. Sung, "Sparse blind carrier-frequency offset estimation for OFDMA uplink," *IEEE Transactions on Communications*, vol. 64, no. 12, pp. 5254–5265, 2016.
- [8] M. Huang, L. Huang, C. Guo, P. Zhang, J. Zhang, and L. Yang, "Carrier frequency offset estimation in uplink OFDMA systems: An approach relying on sparse recovery," *IEEE Transactions on Vehicular Technology*, vol. 66, no. 10, pp. 9592–9597, 2017.
- [9] H. Abdzadeh-Ziabari, W. Zhu, and M. N. S. Swamy, "Joint maximum likelihood timing, frequency offset, and doubly selective channel estimation for OFDM systems," *IEEE Transactions on Vehicular Technology*, vol. 67, no. 3, pp. 2787–2791, 2018.
- [10] R. Shaked, N. Shlezinger, and R. Dabora, "Joint estimation of carrier frequency offset and channel impulse response for linear periodic channels," *IEEE Transactions on Communications*, vol. 66, no. 1, pp. 302–319, 2018.
- [11] A. A. Nasir, S. Durrani, H. Mehrpouyan, S. D. Blostein, and R. A. Kennedy, "Timing and carrier synchronization in wireless communication systems: a survey and classification of research in the last 5 years," *EURASIP Journal on Wireless Communications and Networking*, vol. 2016, no. 1, p. 180, 2016.
- [12] D. Chang, "Effect and compensation of symbol timing offset in OFDM systems with channel interpolation," *IEEE Transactions on Broadcasting*, vol. 54, no. 4, pp. 761–770, 2008.
- [13] M. M. U. Gul, X. Ma, and S. Lee, "Timing and frequency synchronization for OFDM downlink transmissions using Zadoff-Chu sequences," *IEEE Transactions on Wireless Communications*, vol. 14, no. 3, pp. 1716–1729, 2015.
- [14] M. sonal, "Machine learning for PAPR distortion reduction in OFDM systems," 2016.
- [15] T. Van Luong, Y. Ko, N. A. Vien, D. H. Nguyen, and M. Matthaiou, "Deep learning-based detector for OFDM-IM," *IEEE Wireless Communications Letters*, vol. 8, no. 4, pp. 1159–1162, 2019.
- [16] A. Li, Y. Me, S. Xue, N. Yi, and R. Tafazolli, "A carrier-frequency-offset resilient OFDMA receiver designed through machine deep learning," in *2018 IEEE 29th Annual International Symposium on Personal, Indoor and Mobile Radio Communications (PIMRC)*. IEEE, 2018, pp. 1–6.
- [17] Z. He and X. Huang, "Improved deep learning in OFDM systems with imperfect timing synchronization," in *2020 IEEE 91st Vehicular Technology Conference (VTC2020-Spring)*. IEEE, 2020, pp. 1–5.
- [18] S. Dörner, S. Cammerer, J. Hoydis, and S. t. Brink, "Deep learning based communication over the air," *IEEE Journal of Selected Topics in Signal Processing*, vol. 12, no. 1, pp. 132–143, 2018.
- [19] H. Wu, Z. Sun, and X. Zhou, "Deep learning-based frame and timing synchronization for end-to-end communications," in *Journal of Physics: Conference Series*, vol. 1169, no. 1, 2019, p. 012060.
- [20] C. Qing, W. Yu, B. Cai, J. Wang, and C. Huang, "ELM-based frame synchronization in burst-mode communication systems with nonlinear distortion," *IEEE Wireless Communications Letters*, vol. 9, no. 6, pp. 915–919, 2020.
- [21] V. Ninkovic, D. Vukobratovic, A. Valka, and D. Dumic, "Deep learning based packet detection and carrier frequency offset estimation in IEEE 802.11ah," *arXiv preprint arXiv:2004.11716*, 2020.
- [22] C. E. Shannon, "A mathematical theory of communication," *The Bell System Technical Journal*, vol. 27, no. 3, pp. 379–423, 1948.
- [23] J. Liu, K. Mei, X. Zhang, D. Ma, and J. Wei, "Online extreme learning machine-based channel estimation and equalization for OFDM systems," *IEEE Communications Letters*, vol. 23, no. 7, pp. 1276–1279, jul 2019.
- [24] Y. S. Cho, J. Kim, W. Y. Yang, and C. G. Kang, *MIMO-OFDM wireless communications with MATLAB*. John Wiley & Sons, 2010.
- [25] J. . van de Beek, O. Edfors, M. Sandell, S. K. Wilson, and P. O. Borjesson, "On channel estimation in OFDM systems," in *1995 IEEE 45th Vehicular Technology Conference. Countdown to the Wireless Twenty-First Century*, vol. 2, 1995, pp. 815–819 vol.2.
- [26] T. Kim and T. Adali, "Approximation by fully complex multilayer perceptrons," *Neural Computation*, vol. 15, no. 7, pp. 1641–1666, 2003.
- [27] T. Schenk, *RF imperfections in high-rate wireless systems: impact and digital compensation*. Springer Science & Business Media, 2008.



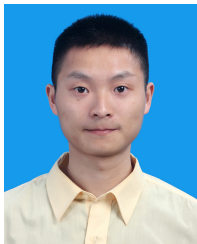
**Jun Liu** received the B.S. degree in optical information science and technology from the South China University of Technology (SCUT), in 2015, and the M.E. degree in communications and information engineering from the National University of Defense Technology (NUDT), Changsha, China, in 2017, where he is currently pursuing the Ph.D. degree with the Department of Cognitive Communications.

He is currently a visiting Ph.D. student with the University of Leeds. His current research interests include machine learning with a focus on shallow neural networks applications, signal processing for broadband wireless communication systems, multiple antenna techniques, and wireless channel modeling.



**Dongtang Ma** (SM'13) received the B.S. degree in applied physics and the M.S. and Ph.D. degrees in information and communication engineering from the National University of Defense Technology (NUDT), Changsha, China, in 1990, 1997, and 2004, respectively. From 2004 to 2009, he was an Associate Professor with the College of Electronic Science and Engineering, NUDT. Since 2009, he is a professor with the department of cognitive communication, School of Electronic Science and Engineering, NUDT. From Aug. 2012 to Feb. 2013,

he was a visiting professor at University of Surrey, UK. His research interests include wireless communication and networks, physical layer security, intelligent communication and network. He has published more than 150 journal and conference papers. He is one of the Executive Directors of Hunan Electronic Institute. He served as the TPC member of PIMRC from 2012 to 2020.



**Kai Mei** received the master's degree from the National University of Defense Technology, in 2017, where he is currently pursuing the Ph.D. degree. His research interests include synchronization and channel estimation in OFDM systems and MIMO-OFDM systems, and machine learning applications in wireless communications.



**Jibo Wei** (Member, IEEE) received the B.S. and M.S. degrees from the National University of Defense Technology (NUDT), Changsha, China, in 1989 and 1992, respectively, and the Ph.D. degree from Southeast University, Nanjing, China, in 1998, all in electronic engineering. He is currently the Director and a Professor of the Department of Communication Engineering, NUDT. His research interests include wireless network protocol and signal processing in communications, more specially, the areas of MIMO, multicarrier transmission, cooperative communication, and cognitive network. He is a member of the IEEE

Communication Society and also a member of the IEEE VTS. He also works as one of the editors of the Journal on Communications and is a Senior Member of the China Institute of Communications and Electronics.



**Xiaochen Zhang** is currently a graduate student at College of Electronic Science and Engineering from National University of Defense Technology (NUDT), Changsha, China. He received the B.S. degree from NUDT in 2018. His research interests include resource allocation, multi-access edge computing, machine learning and channel modeling.



**Syed Ali Raza Zaidi** (Senior Member, IEEE) is currently a University Academic Fellow (Assistant Professor) in the broad area of Communication and Sensing for RAS. He was awarded J. W. and F. W. Carter Prize, was also awarded with COST IC0902, EPSRC, DAAD and Royal Academy of Engineering grants. He has published more than 100 technical papers in various top-tier IEEE Journals and conferences. His research interests include design and implementation of communication protocols for wireless networking specifically in the area of M2M.



**Des McLernon** (Member, IEEE) received his B.Sc and MSc degrees from the Queen's University of Belfast, N. Ireland. After working on radar systems research with Ferranti Ltd in Edinburgh, Scotland, he then joined Imperial College, University of London, UK, where he took his PhD in signal processing. His research interests are broadly within the domain of signal processing for wireless communications in which field he has published around 340 journal and conference papers. Finally, in what spare time remains, he plays jazz piano in restaurants and bars

and was recently runner-up in the 2018 "Leeds Pub Piano" competition.